ACS APPLIED ELECTRONIC MATERIALS

Made available for a limited time for personal research and study only License.

pubs.acs.org/acsaelm Article

Controlling the Wet-Etch Directionality in Nanostructured Silicon

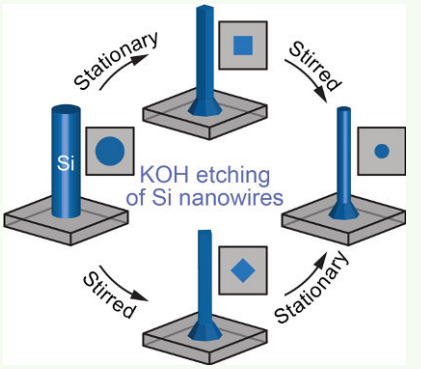
Zainul Aabdin, Tanmay Ghosh, Antoine Pacco, Sanoj Raj, Hue Thi Bich Do, Khakimjon Saidov, Tjiu Weng Weei, Utkarsh Anand, Petr Král, Frank Holsteyns, Michel Bosman,* and Utkur Mirsaidov*

Cite This: ACS Appl. Electron. Mater. 2022, 4, 5191−5198

Read Online

ACCESS | Metrics & More | Article Recommendations | Supporting Information

ABSTRACT: Anisotropic wet etching of crystalline silicon (c-Si) is a key chemical process used in microelectronic device fabrication. Controlled fabrication of c-Si nanostructures requires an understanding of how crystal planes evolve during silicon etching. Here, by imaging KOH wet etching of c-Si nanowires, we show that it is possible to switch the fast-etching direction (i.e., the etch anisotropy) between the Si {100} and {110} crystal planes at will through mechanical agitation of the etchant. Based on molecular dynamics simulations, we attribute this switching to the higher affinity of the $Si(OH)_4$ etch byproducts to the Si {110} planes. These surface-bound byproducts hinder etchant access to the {110} surfaces under stationary etching conditions and thus reduce the etch rate in ⟨110⟩ directions. Most importantly, by cycling through stirred and stationary modes of etching, we can obtain isotropic etch profiles, fabricating high-quality, round Si nanowires with sub-10 nm diameters. Our study provides an important insight into the nanoscale wet etching of Si and demonstrates a new level of control for enabling highly scalable, advanced nanoelectronic devices.



KEYWORDS: *Si, Chemical Etching, Nanostructures, Nanowires, Nanofabrication, In situ TEM*

Downloaded via UNIV OF ILLINOIS CHICAGO on December 23, 2022 at 23:17:19 (UTC).
See https://pubs.acs.org/sharingguidelines for options on how to legitimately share published articles.

INTRODUCTION

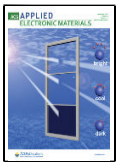
Modern microprocessors comprising billions of precisely engineered Si transistors rely on advanced semiconductor nanofabrication. To keep up with the demand for faster and more efficient microprocessors, their performance is boosted by continuously increasing the on-chip density of the transistors.[1] In previous and current generations of planar and fin-shaped field-effect transistors (FinFETs), the increase in density is typically achieved by reducing the lateral transistor dimensions.[2,3] While this approach to scaling worked very well in the past, it is reaching its limit, with critical transistor dimensions nearing only a few tens of atoms.[4,5] To overcome the limitations of this classical dimensional scaling, the transistor architecture is being changed into stacked horizontal and vertical gate-all-around field-effect transistors (GAA-FETs),[6,7] requiring new fabrication processes.[8,9]

Three-dimensional (3D) Si nanostructures, including vertical nanowires, are produced by plasma-based dry reactive ion etching.[10] However, dry etching has a fundamental limitation: the unavoidable damage to the surface caused by energetic ions, which becomes a limiting factor on device performance.[11,12] In contrast to dry etching, wet chemical etching does not cause a rough and structurally damaged surface, as the surface atoms are removed through a direct chemical reaction with the etchant. Furthermore, as an industrial process, wet etching is advantageous as it can process more wafers at once and etches more uniformly than dry etching.[13,14]

The two most commonly used solutions for wet chemical etching of c-Si are potassium hydroxide (KOH) and tetramethylammonium hydroxide (TMAH). The key issue with both of these alkaline solutions is that they etch Si anisotropically: with nonidentical etch rates along different crystallographic directions.[15−18] While directionally different etch rates are used to generate unique 3D structures, such as trenches,[19−21] surface texture,[22,23] macropores,[24] and cantilevers,[25−27] anisotropic etching prevents the fabrication of circular vertical nanowires needed for future GAAFETs. Wet etching of c-Si can be modified by adding metal impurities,[28,29] alcohols,[30−32] or by using acoustic,[33] optical,[34] or microwave[35,36] irradiation, but so far, no method is available for controllable switching of the etch anisotropy.

Here, we demonstrate selective switching of the fast- and slow-etching directions in Si to obtain nanoscale control over the exact shape of the designed structures. Using an *in situ* liquid-phase TEM platform, we visualize the dynamics of Si wet etching with nanometer precision. Our simple method switches the fast-etching directions between the Si {100} and {110} crystal planes by controlling the diffusion of etch

Received: June 26, 2022
Accepted: October 16, 2022
Published: November 12, 2022



ACS Publications © 2022 American Chemical Society

https://doi.org/10.1021/acsaelm.2c00824
ACS Appl. Electron. Mater. 2022, 4, 5191−5198

byproducts away from the surface through mechanical agitation during the etching. Using this approach, we show that we can produce sub-10 nm diameter monocrystalline vertical Si nanowires with circular profiles instead of the usual anisotropic square profiles. The new level of design control that this method provides is expected to form an important step in the realization of vertical GAAFETs.

RESULTS

Our experimental platform for testing the wet etching of c-Si nanowires in alkaline solutions is shown in Figure 1. It consists of a densely packed array of (001) cylindrical Si nanowires fabricated on top of a free-standing 145-nm-thick SiO_2 film (Supporting Information Section 1). Figure 2 shows results from *in-flask* studies describing how the nanowires evolve when etched in 1% (w/v) KOH solution at room temperature.

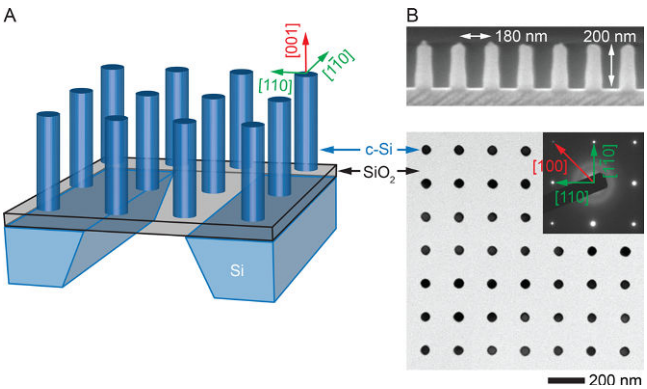


Figure 1. Overview of c-Si nanowires test structure. (A) Schematic illustration of a test chip used for etching studies. (B) Side-view SEM (upper panel) and top-down TEM (lower panel) images showing a 7 × 7 array of equally spaced c-Si nanowires. The nanowires are 45 ± 5 nm in diameter with a center-to-center spacing of 180 nm. The selected area electron diffraction in the inset of the lower panel shows that the nanowires are monocrystalline, and all of them are oriented in the [001] direction such that the array diagonal represents the [100] direction.

Under stationary etching conditions (i.e., while keeping the nanowires still), the sidewalls of the Si nanowires quickly evolve to be {100}-faceted, as shown in Figure 2B. These square profiles are maintained all the way until the nanowires are fully etched in the solution. In contrast to Figure 2B, Figure 2C shows the wet etching under the exact same conditions, but now while "stirring," meaning the chip with the Si nanowires was continuously moved back and forth (and parallel to the wafer plane) inside the solution, throughout the etching process, as described in more detail in Supporting Information Section 2. Here, at the initial stages of the etching, we observed a roughening of the nanowire sidewalls (t = 5 s) into multiple low- and high-index crystal planes. As etching progressed, Si {110} facets started to develop, indicating that ⟨110⟩ is now the fast etching direction. To quantitatively assess the switching of the etch anisotropy, we measured the Si etch rates along the ⟨100⟩ directions without stirring to be 1.0 ± 0.3 nm s^{-1}, and in the ⟨110⟩ directions in the stirred case to be 5.4 ± 0.5 nm s^{-1} (Figure 2D,E). These are unexpected observations, and controllable rotation of the fast-etching direction by 45°, to our best knowledge, has not been observed before.

Si etching is well-studied for higher concentrations (10−60% (w/v)) of KOH and elevated temperatures (70−90 °C).[17,18,37,38] However, KOH etching at low concentrations and low temperatures (i.e., similar to conditions used in our study) has not been carefully examined in the past. While stationary etching of Si is known to result in slower etch rates compared to stirred etching,[17,38] no switching of the etch anisotropy has yet been reported. However, these studies used a magnetic stirrer to agitate the KOH solution,[17,38] which is different from our case, where stirring is achieved by rocking the sample in a preferred direction. When the sample is rocked back and forth along the ⟨110⟩ direction (i.e., parallel to (001) planes) in KOH solution, the etch directionality switches. Furthermore, the square (and not rectangular) profile of the nanowires observed after stirring indicates that the fluid flow dynamics does not affect the etching of different facets.

In order to rule out the effects of any possible artifact such as the formation of nanobubbles in the solution or only partial

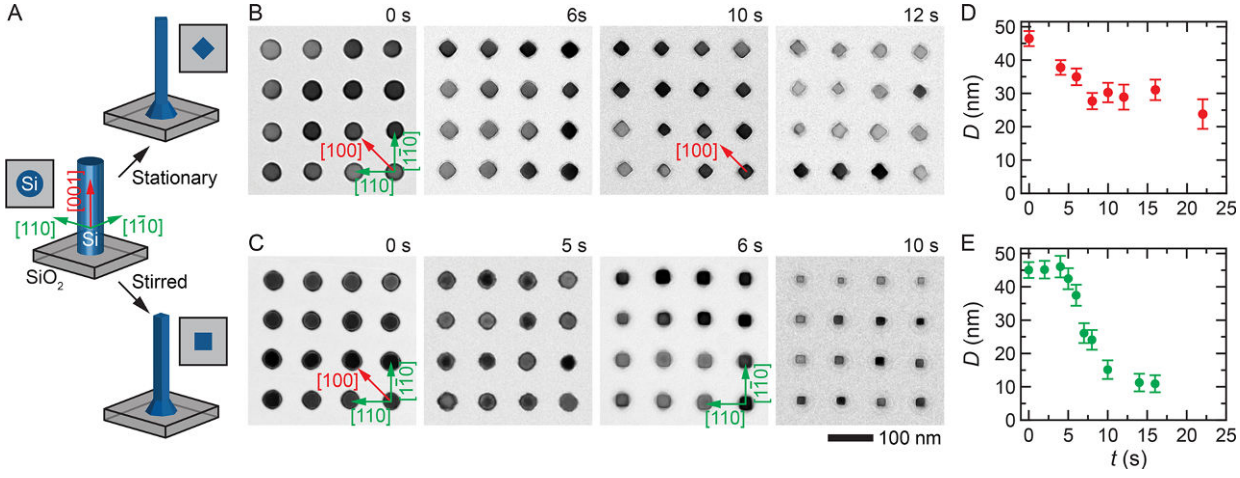


Figure 2. Effect of stirring on the c-Si wet-etch anisotropy. (A) Schematic illustration of the nanowires etch profiles after stationary and stirred etching. TEM images showing *in-flask* (B) stationary and (C) stirred etching of c-Si nanowires in 1% (w/v) KOH solution at room temperature obtained by quenching the etch reactions at different time points (see Figures S7 and S8 for detailed image series). These TEM images show that the stationary etching process produces {100}-faceted nanowires, whereas the stirred etching produces the {110}-faceted nanowires. The average width (D) of the nanowires along (D) ⟨100⟩ and (E) ⟨110⟩ directions as a function of time for stationary and stirred etching cases, respectively.

https://doi.org/10.1021/acsaelm.2c00824
ACS Appl. Electron. Mater. 2022, 4, 5191−5198

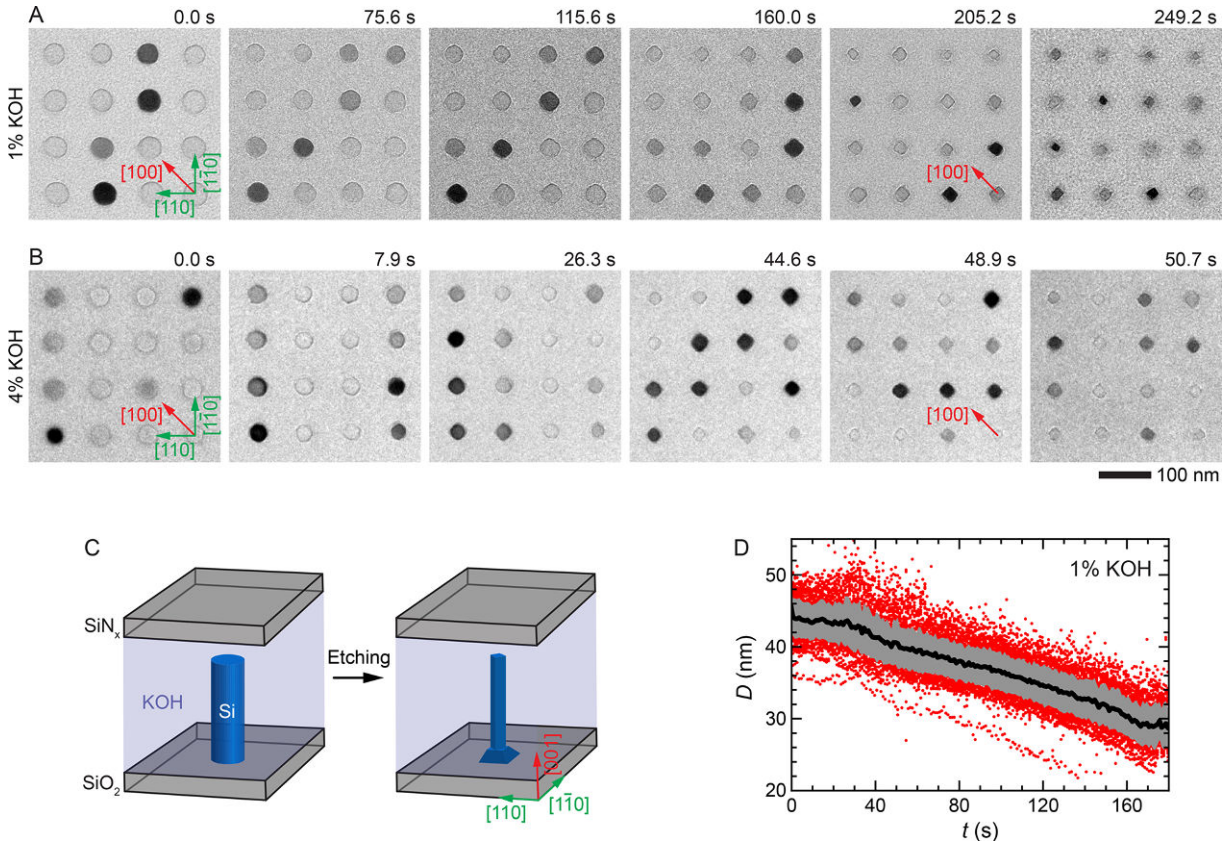


Figure 3. Evolution of the facets during *in situ* etching of c-Si nanowires. A series of *in situ* TEM images showing real-time etching of c-Si nanowires in (A) 1% and (B) 4% (w/v) KOH solutions at room temperature (SI Videos 1 and 2). (C) Schematic illustration of the nanowires in a liquid cell during *in situ* TEM imaging, showing the formation of {100} facets. (D) Measured width (D) of individual nanowires along the Si ⟨100⟩ directions as a function of time (red points) when etched in 1% (w/v) KOH solution. The solid black line and gray region show the average and one standard deviation of these points, respectively. Supporting Information Section 3 describes the image processing used for extracting the widths of nanowires.

wetting of the nanowire surfaces that may cause the observed 45°-rotation of fast etching direction, we imaged the etching of these nanowires in real-time using our custom-designed *in situ* liquid cell TEM platform (Supporting Information Sections 1 and 2). Since the electron beam can affect the etching during TEM imaging,[39−42] we reduced the electron flux to <25 e Å^{-2} s^{-1} to minimize these effects on the etching process, as described in our earlier study.[39] Similar to the *in-flask* result in Figure 2B, our *in situ* experiments show the development of facets along the Si {100} planes (Figure 3A,B). More importantly, throughout the etching, the nanowires remained fully immersed in the etchant, and no bubbles were formed. The only difference between the *in situ* (Figure 3A,B) and *in-flask* (Figure 2B) observations is that the *in situ* etch rate is significantly lower. The average *in situ* etch rate for the Si ⟨100⟩ directions was 0.10 ± 0.02 nm s^{-1} and 0.21 ± 0.04 nm s^{-1} for 1% and 4% (w/v) KOH concentrations, respectively (Figure 3D). These slower *in situ* etch rates can be explained by the quick depletion of hydroxyl ions (OH^-) in the KOH solutions as they react with the SiO_2 support film (Figure S9).[17,39] The depletion of hydroxyl ions results from the confined volume of the liquid cell, which slows the diffusion of etchant molecules, effectively reducing the strength of the etchant; hence the associated etch rates decrease. This is in contrast to the *in-flask* experiments, where the bulk amount of KOH solution in a beaker prevents the depletion of the hydroxyl ions near the etching surfaces. Nevertheless, despite the difference in etch rates, the evolution of the stationary etch profiles is similar for both the *in situ* and *in-flask* observations. Therefore, we safely rule out the formation of nanobubbles or partial wetting to be the cause of the observed etch profiles.

To explain the observed switching of the etching directions, we hypothesize that the key factor that controls the directional etch rates is the reaction byproducts that form and accumulate on the Si surface, which, in turn, block access to hydroxyl ions responsible for the etching. During KOH etching of Si, $Si(OH)_4$ is the only primary reaction byproduct.[43,44] This fact allows us to relatively simply extend the atomistic molecular dynamics (MD) simulations that were earlier used to describe the etching of amorphous Si nanopillars[39] to c-Si nanowires (Supporting Information Section 4). Our simulated system shown in Figure 4 comprises uniformly distributed $Si(OH)_4$ molecules on partially hydroxyl-terminated Si surfaces (Figures 4A−D). For both Si {100} and {110} planes, the simulations show that when the surfaces in KOH solution are subjected to an oscillatory movement that mimics the etching conditions for the stirred case, etch byproducts are transported away from the surface (Figures 4G,H). Conversely, when the surfaces are stationary in the solution, removal of the byproducts via diffusion is significantly slower (Figures 4E−F). In addition, there is a marked difference between the rate at which byproducts are removed from the two planes under the stirred and stationary conditions (Figures 4J and S6C). In the stirred case (with an oscillatory force of 21 pN), the removal rate of

https://doi.org/10.1021/acsaelm.2c00824
ACS Appl. Electron. Mater. 2022, 4, 5191−5198

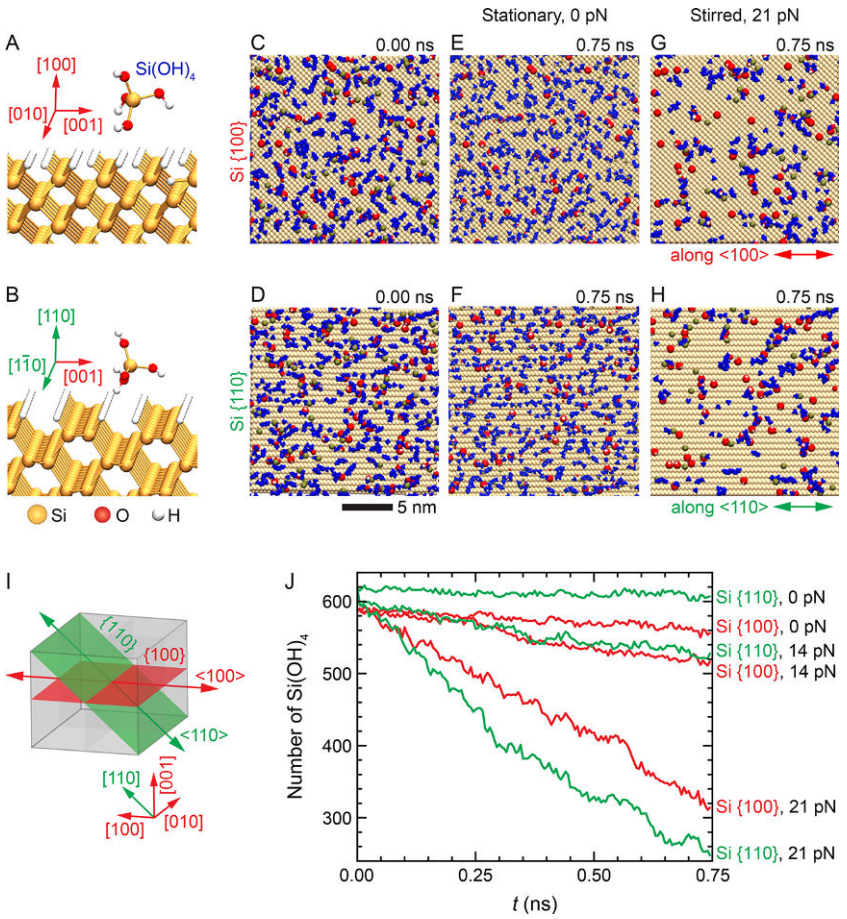


Figure 4. Molecular dynamics simulations of etch byproducts on a Si surface. Atomic-scale view of (A) Si {100} and (B){110} planes showing how $Si(OH)_4$ interacts with these surfaces. Atomistic MD simulations showing the aggregation (t = 0 ns) of 936 $Si(OH)_4$ molecules (blue) on (**C**) Si {100} and (**D**) Si {110} planes (yellow) terminated with 5% OH^- (red) and 95% H (white balls in (A) and (B)). Free OH^- and K^+ ions are shown as small red and olive color balls, respectively. Water molecules and ions are not shown for clarity. Remaining $Si(OH)_4$ molecules on stationary (E) Si {100} and (F) {110} surfaces after 0.75 ns (i.e., no stirring force is applied, 0 pN). $Si(OH)_4$ molecules on (G) Si {100} and (H) {110} surfaces stirred with oscillatory force of 21 pN applied along ⟨100⟩ and ⟨110⟩ directions, respectively. (I) Schematic illustration of Si {100} (red) and {110} (green) planes and their respective stir directions indicated with red and green arrows. (J) The number of $Si(OH)_4$ molecules that remain on the Si {100} and {110} surfaces as a function of time for stationary surfaces (0 pN) and the surface stirred with oscillatory forces of 14 and 21 pN.

the byproducts from Si {110} is higher, whereas in the stationary case (0 pN), the removal rate of the $Si(OH)_4$ byproducts from Si {110} surface is lower. This is because the byproduct binds stronger to this surface (7.1 kcal mol^{-1}) than to Si {100} surface (4.7 kcal mol^{-1}), as obtained from our MD simulations (Supporting Information Section 4).

Hence, we conclude that under stationary etching conditions, access of the etchant to and removal of the etch byproducts from {110} planes is hindered more than for the {100} planes, which, in turn, can be held responsible for the observed slower etch rates in the ⟨110⟩ directions. To test this experimentally, we conducted wet etching in TMAH solution, which is known to sterically shield the Si surface and inhibit the formation of etch byproduct clusters.[39,43] As expected, no switching in etch anisotropy was observed when the nanowires were etched in TMAH solution both under stirred and stationary conditions (Figures S10–S12).

Combining these insights, we next demonstrate the capability to etch c-Si nanowires into the nanowires with circular cross sections, which is only achievable with full control over anisotropic etching. It must be noted that for our Si nanowires, the etchant will inadvertently etch the nanostructures from the top, shortening them. To prevent this, we used Si nanowires with a 30-nm-thick SiN_x film cap (Figure 5A) and verified that capping does not affect the observed anisotropy both for stirred (Figure 5B) and stationary (Figure 5C) etching processes, except that it creates the expected shoulder at the top SiN_x interface. Controlled switching between stationary and stirred etching conditions makes it now possible to switch the etching direction from the {110} to the {100} planes, as shown in Figure 5A–C. Figure 5D shows the nanowire array obtained after 4 s of stirred etching, followed by 5 s of stationary etching. The circular top-down profiles reveal that the resulting nanowires are indeed cylindrical.

So far, our discussion of etch rates was limited to ⟨110⟩ and ⟨100⟩ directions. To understand why instead of the expected octagonal nanowires (schematic in Figure 5D), cylindrical nanowires (TEM image in Figure 5D) were produced, we have to account for the fact that etching occurs along all the crystal directions, albeit at different rates, as summarized in Figure S14. Moreover, the duration for both the stationary and stirred etching used in our combined etching means that well-defined nanoscale facets are dynamically evolving, favoring the overall isotropic etch profile, which produces cylindrical nanowires.

https://doi.org/10.1021/acsaelm.2c00824
ACS Appl. Electron. Mater. 2022, 4, 5191−5198

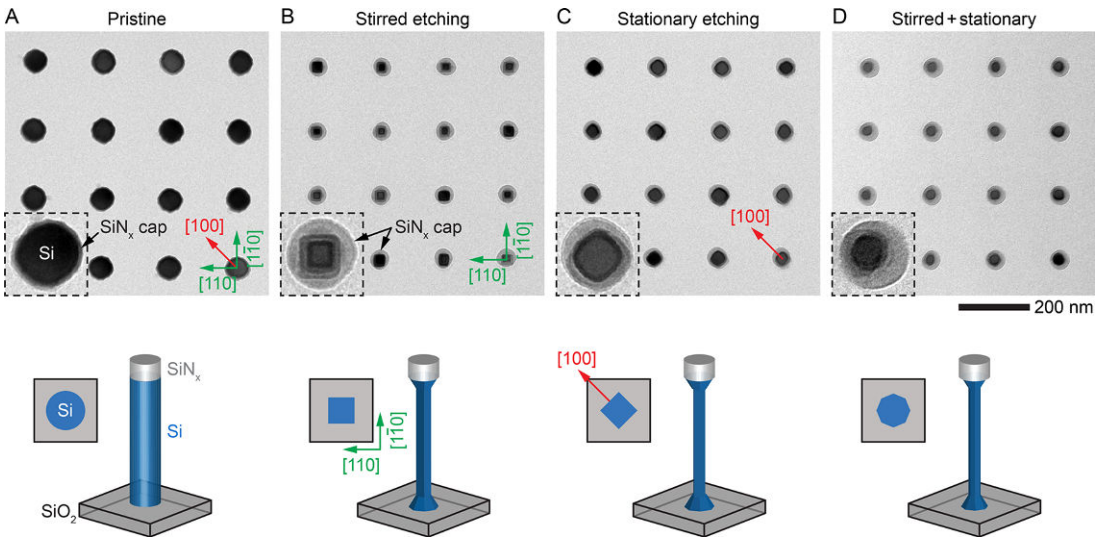


Figure 5. Achieving cylindrical nanowire profile via cycled etching. A series of TEM images (upper panels) and schematic illustration of expected etch profiles (lower panels) showing how cycling between stationary and stirred etching in 2% (w/v) KOH solution can produce narrower nanowires with a circular profile: (A) pristine nanowires, (B) nanowires after 10-s-long stirred etching, (C) nanowires after 10-s-long stationary etching, and (D) nanowires after 4 s long stirred etching, followed by 5 s long stationary etching. Here, nanowires are capped with SiN_x film to prevent any etching from the top. The insets in the TEM images show a zoomed-in view of individual nanowires for each case.

The uniform TEM contrast throughout the widths of the etched nanowires indicates that their surfaces remain of good monocrystalline quality. Hence our approach presents a unique technique for fabricating very thin, monocrystalline Si nanowires with circular cross sections. This meets the key fabrication requirement for functional electron channels in the next-generation vertical GAAFETs.[45−47]

CONCLUSIONS

This study provides a direct insight into the dynamics of wet chemical etching of c-Si nanostructures. We show that it is possible to controllably switch the fast-etching directions between the ⟨100⟩ and ⟨110⟩ crystallographic orientations. Moreover, by regulating the mechanical agitation of the Si nanostructures during the etching, we demonstrate a simple method to achieve an isotropic profile and fabricate cylindrical nanowires, a critical step in the advancement of future-generation nanowire-based Si transistor architectures. More broadly, our *in situ* TEM approach to observing wet-etch dynamics at the nanoscale lays the foundation for further studies that will help to gain new insight into the dynamics of chemical processes at the nanoscale.

MATERIALS AND METHODS

Materials. Etching solutions were prepared from the following chemicals: KOH pellets (85% purity, Cat. No. 306568, Sigma-Aldrich Co. LLC, St. Louis, U.S.A.), TMAH solution (25 wt %, Cat. No. 331635, VWR International LLC, Radnor, PA, U.S.A.), and HF solution (48 wt %, Cat. No. 339261, Sigma-Aldrich Co. LLC, St. Louis, U.S.A.). We used ACS-grade water (Cat. No. 320072, Sigma-Aldrich Co. LLC, St. Louis, U.S.A.) to prepare all the solutions used in this study.

Fabrication of Devices. Test samples of c-Si nanowires were fabricated on 300 mm standard Si -on-insulator (SOI) wafers using immersion lithography techniques (Figure S1A).[48,49] The SOI wafer consists of a 775-μm-thick Si handle wafer, a 145-nm-thick SiO_2 film, and a device layer of c-Si on top of the SiO_2 film. SiN_x layers (30 nm) were deposited on both sides of the wafer, which served as a hard mask during dry and wet etching. Different aspect-ratio nanowires were fabricated using suitable device layer thicknesses (Figure S2).

Then, these 300 mm wafers were diced into smaller pieces measuring 72 × 72 mm^2, which were used for the fabrication of chips with nanowires (Figure S1B). Central viewing windows and grooves for cleaving individual chips were patterned on the backside SiN_x layer using a conventional photolithography process, followed by deep reactive ion etching (DRIE) of the exposed SiN_x. After the DRIE, the exposed Si was etched from the backside of the wafer in a 30% (w/v) KOH solution, releasing the SiO_2 membrane. The SiO_2 membrane was thinned down from 145 to 45 nm by etching in 5 wt % TMAH. The lateral dimensions of individual chips were 4 × 5 mm^2 with electron transparent SiO_2 viewing membrane windows in the center with the size of 30 × 70 μm^2 (for TEM imaging). The front side of the wafer with the nanowires was protected using a physical chuck during the entire microfabrication process and was kept out of contact with the photoresist, the KOH and TMAH solutions, and the rinse liquids to avoid contamination and damage to the fragile Si nanowires. The detailed steps of the fabrication process are described in Supporting Information Section 1.

Imaging. All *in-flask* etching experiments were done at room temperature (22 °C) in a controlled manner using a custom-built robotic arm (Figure S3), programmed to perform the etching in a series of three automated steps: (i) etching, (ii) quenching, and (iii) rinsing. After drying the rinsed samples, they were imaged using a custom-built retainer for static liquid cells in a JEOL2010F TEM (JEOL Ltd. Akishima, Tokyo, Japan) operating at 200 kV and equipped with a OneView CMOS camera (Gatan, Inc., Pleasanton, CA, U.S.A.).

For *in situ* liquid phase TEM studies, we assembled and loaded a dry sample into a custom-built liquid-flow TEM holder (Figure S4), which was then inserted into the TEM for imaging. Once the sample was loaded and ready for imaging, KOH solution was flown at a rate of 5−10 $\mu L\ min^{-1}$. To minimize any adverse effect of the electron beam on the sample during imaging, a low electron flux of <25 e $Å^{-2}\ s^{-1}$ was used,[39] and 2048 × 2048 pixels-size movies were recorded at a rate of 5−10 frames per second. Details of the imaging and image analysis used in this study are described in Supporting Information Sections 2−3.

Atomistic MD simulations. The MD simulations were performed with Nanoscale Molecular Dynamics (NAMD) software package,[50] using the Chemistry at Harvard Macromolecular Mechanics (CHARMM) general force field.[51] The systems were simulated in an NPT ensemble at T = 300 K, using the Langevin dynamics with a damping constant of γ_{Lang} = 0.1 ps^{-1} and a time step

https://doi.org/10.1021/acsaelm.2c00824
ACS Appl. Electron. Mater. 2022, 4, 5191−5198

of 2 fs. The CHARMM general force field was implemented for the bond, angle, and dihedral parameters of the ions and water molecules. $Si(OH)_4$ and Si parameters were taken from our earlier publication.[39] Nonbonding interactions between these molecules, such as a van der Waals (vdW) attraction and a steric repulsion, were described by the Lennard–Jones (LJ) potential (eq 1)

$$U_{LJ}(r) = \varepsilon\left[\left(\frac{r_{min}}{r}\right)^{12} - 2\left(\frac{r_{min}}{r}\right)^{6}\right] \quad (1)$$

Here, ε is the minimum (negative) energy of this coupling, and r_{min} is the distance where $U_{LJ}(r)$ has a local minimum. In NAMD, the LJ potential has a typical cutoff distance of 1 nm (within the water). The electrostatic interaction between ions and partially charged atoms has a similar cutoff, but its long-range part (beyond the cutoff distance) was calculated by the Particle Mesh Ewald (PME) method in the presence of periodic boundary conditions.[52] Further details describing the parameters of the simulation can be found in Supporting Information Section 4.

■ ASSOCIATED CONTENT

Supporting Information

The authors declare no competing interests. The Supporting Information is available free of charge at https://pubs.acs.org/doi/10.1021/acsaelm.2c00824.

In situ TEM video showing etching of c-Si nanowires in 1% (w/v) KOH solution at 22 °C, as described in Figure 3A (AVI)

In situ TEM video showing etching of c-Si nanowires in 4% (w/v) KOH solution at 22 °C, as described in Figure 3B and Figure S9 (AVI)

Methods, additional experiments, and MD simulations (PDF)

■ AUTHOR INFORMATION

Corresponding Authors

Utkur Mirsaidov − *Centre for BioImaging Sciences and Department of Biological Sciences, National University of Singapore, 117557, Singapore; Department of Physics, National University of Singapore, 117551, Singapore; Department of Materials Science and Engineering, National University of Singapore, 117575, Singapore; Centre for Advanced 2D Materials and Graphene Research Centre, National University of Singapore, 117546, Singapore;* orcid.org/0000-0001-8673-466X; Email: mirsaidov@nus.edu.sg

Michel Bosman − *Institute of Materials Research and Engineering, Agency for Science, Technology and Research (A*STAR), 138634, Singapore; Department of Materials Science and Engineering, National University of Singapore, 117575, Singapore;* orcid.org/0000-0002-8717-7655; Email: msemb@nus.edu.sg

Authors

Zainul Aabdin − *Institute of Materials Research and Engineering, Agency for Science, Technology and Research (A*STAR), 138634, Singapore; Centre for BioImaging Sciences and Department of Biological Sciences, National University of Singapore, 117557, Singapore;* orcid.org/0000-0002-0436-1327

Tanmay Ghosh − *Centre for BioImaging Sciences and Department of Biological Sciences, National University of Singapore, 117557, Singapore; Department of Physics, National University of Singapore, 117551, Singapore;* orcid.org/0000-0003-0532-2407

Antoine Pacco − *imec, B-3001 Leuven, Belgium*

Sanoj Raj − *Department of Chemistry, University of Illinois at Chicago, Chicago, Illinois 60607, United States*

Hue Thi Bich Do − *Institute of Materials Research and Engineering, Agency for Science, Technology and Research (A*STAR), 138634, Singapore; Department of Materials Science and Engineering, National University of Singapore, 117575, Singapore*

Khakimjon Saidov − *Centre for BioImaging Sciences and Department of Biological Sciences, National University of Singapore, 117557, Singapore; Department of Physics, National University of Singapore, 117551, Singapore; Centre for Advanced 2D Materials and Graphene Research Centre, National University of Singapore, 117546, Singapore;* orcid.org/0000-0003-1809-4706

Tjiu Weng Weei − *Institute of Materials Research and Engineering, Agency for Science, Technology and Research (A*STAR), 138634, Singapore*

Utkarsh Anand − *Centre for BioImaging Sciences and Department of Biological Sciences, National University of Singapore, 117557, Singapore; Department of Physics, National University of Singapore, 117551, Singapore;* orcid.org/0000-0003-3914-8435

Petr Král − *Department of Chemistry and Departments of Physics, Pharmaceutical Sciences, and Chemical Engineering, University of Illinois at Chicago, Chicago, Illinois 60607, United States;* orcid.org/0000-0003-2992-9027

Frank Holsteyns − *imec, B-3001 Leuven, Belgium*

Complete contact information is available at: https://pubs.acs.org/10.1021/acsaelm.2c00824

Notes

The authors declare no competing financial interest.

■ ACKNOWLEDGMENTS

This work was supported by Singapore's National Research Foundation (NRF) under the Competitive Research Programme (NRFCRP16-2015-05).

■ REFERENCES

(1) Waldrop, M. M. The chips are down for Moore's law. *Nature* **2016**, *530* (7589), 144−147.

(2) El-Atab, N.; Hussain, M. M.The future of CMOS: More Moore or a new disruptive technology? In *Advanced Nanoelectronics*, 1st ed.; Wiley-VCHVerlag GmbH & Co. KGaA: Germany, 2018; pp 1−31.

(3) Radamson, H. H.; He, X.; Zhang, Q.; Liu, J.; Cui, H.; Xiang, J.; Kong, Z.; Xiong, W.; Li, J.; Gao, J.; Yang, H.; Gu, S.; Zhao, X.; Du, Y.; Yu, J.; Wang, G. Miniaturization of CMOS. *Micromachines* **2019**, *10* (5), 293.

(4) Huang, R.; Wang, R.; Zhuge, J.; Liu, C.; Yu, T.; Zhang, L.; Huang, X.; Ai, Y.; Zou, J.; Liu, Y.; Fan, J.; Liao, H.; Wang, Y.Characterization and analysis of gate-all-around Si nanowire transistors for extreme scaling. In *2011 IEEE Custom Integrated Circuits Conference (CICC)*, San Jose, CA, USA, 2011; pp 1−8.

(5) Kuhn, K. J. Considerations for ultimate CMOS scaling. *IEEE Trans. Electron Devices* **2012**, *59* (7), 1813−1828.

(6) Goldberger, J.; Hochbaum, A. I.; Fan, R.; Yang, P. Silicon vertically integrated nanowire field effect transistors. *Nano Lett.* **2006**, *6* (5), 973−977.

(7) Tomioka, K.; Yoshimura, M.; Fukui, T. A III−V nanowire channel on silicon for high-performance vertical transistors. *Nature* **2012**, *488* (7410), 189−192.

(8) Yakimets, D.; Eneman, G.; Schuddinck, P.; Trong, H. B.; Bardon, M. G.; Raghavan, P.; Veloso, A.; Collaert, N.; Mercha, A.; Verkest, D.; Thean, A. V. Y.; De Meyer, K. Vertical GAAFETs for the ultimate CMOS scaling. *IEEE Trans. Electron Devices* **2015**, *62* (5), 1433−1439.
(9) Yin, X.; Zhang, Y.; Zhu, H.; Wang, G. L.; Li, J. J.; Du, A. Y.; Li, C.; Zhao, L. H.; Huang, W. X.; Yang, H.; Xie, L.; Ai, X. Z.; Zhang, Y. B.; Jia, K. P.; Wu, Z. H.; Ma, X. L.; Zhang, Q. Z.; Mao, S. J.; Xiang, J. J.; Gao, J. F.; He, X. B.; Bai, G. B.; Lu, Y. H.; Zhou, N.; Kong, Z. Z.; Zhang, Y.; Zhao, J.; Ma, S. S.; Xuan, Z. H.; Li, Y. Y.; Li, L.; Zhang, Q. H.; Han, J. H.; Chen, R. L.; Qu, Y.; Yang, T.; Luo, J.; Li, J. F.; Yin, H. X.; Radamson, H.; Zhao, C.; Wang, W. W.; Ye, T. C. Vertical sandwich gate-all-around field-effect transistors with self-aligned high-k metal gates and small effective-gate-length variation. *IEEE Electron Device Lett.* **2020**, *41* (1), 8−11.
(10) Donnelly, V. M.; Kornblit, A. Plasma etching: Yesterday, today, and tomorrow. *J. Vac. Sci. Technol. A* **2013**, *31* (5), No. 050825.
(11) Richard, O.; Iacopi, F.; Bender, H.; Beyer, G. Sidewall damage in silica-based low-k material induced by different patterning plasma processes studied by energy filtered and analytical scanning TEM. *Microelectron. Eng.* **2007**, *84* (3), 517−523.
(12) Pang, S. W.Surface damage induced by dry etching. In *Handbook of Advanced Plasma Processing Techniques*; Shul, R. J., Pearton, S. J., Eds.; Springer: Berlin Heidelberg, 2000; pp 309−360.
(13) Taylor, H. K.; Sun, H.; Hill, T. F.; Farahanchi, A.; Boning, D. S. Characterizing and predicting spatial nonuniformity in the deep reactive ion etching of silicon. *J. Electrochem. Soc.* **2006**, *153* (8), C575.
(14) Zhuang, D.; Edgar, J. H. Wet etching of GaN, AlN, and SiC: a review. *Mater. Sci. Eng.: R: Rep.* **2005**, *48* (1), 1−46.
(15) Sato, K.; Shikida, M.; Matsushima, Y.; Yamashiro, T.; Asaumi, K.; Iriye, Y.; Yamamoto, M. Characterization of orientation-dependent etching properties of single-crystal silicon: effects of KOH concentration. *Sens. Actuator A Phys.* **1998**, *64* (1), 87−93.
(16) Sato, K.; Shikida, M.; Yamashiro, T.; Asaumi, K.; Iriye, Y.; Yamamoto, M. Anisotropic etching rates of single-crystal silicon for TMAH water solution as a function of crystallographic orientation. *Sens. Actuator A Phys.* **1999**, *73* (1), 131−137.
(17) Seidel, H.; Csepregi, L.; Heuberger, A.; Baumgärtel, H. Anisotropic etching of crystalline silicon in alkaline solutions: I. Orientation dependence and behavior of passivation layers. *J. Electrochem. Soc.* **1990**, *137* (11), 3612−3626.
(18) Wind, R. A.; Hines, M. A. Macroscopic etch anisotropies and microscopic reaction mechanisms: a micromachined structure for the rapid assay of etchant anisotropy. *Surf. Sci.* **2000**, *460* (1), 21−38.
(19) Ayón, A. A.; Zhang, X.; Khanna, R. Anisotropic silicon trenches 300−500 μm deep employing time multiplexed deep etching (TMDE). *Sens. Actuator A Phys.* **2001**, *91* (3), 381−385.
(20) Ekinci, H.; Dey, R. K.; Cui, B. Two-step potassium hydroxide etching to enhance aspect ratio in trench fabrication. *J. Vac. Sci. Technol. B* **2019**, *37* (6), No. 062001.
(21) Theil, J. A. Deep trench fabrication by Si (110) orientation dependent etching. *J. Vac. Sci. Technol. B Microelectron. Nanometer Struct. Process. Meas. Phenom.* **1995**, *13* (5), 2145−2147.
(22) Papet, P.; Nichiporuk, O.; Kaminski, A.; Rozier, Y.; Kraiem, J.; Lelievre, J.-F.; Chaumartin, A.; Fave, A.; Lemiti, M. Pyramidal texturing of silicon solar cell with TMAH chemical anisotropic etching. *Sol. Energy Mater. Sol. Cells* **2006**, *90* (15), 2319−2328.
(23) Vazsonyi, E.; De Clercq, K.; Einhaus, R.; Van Kerschaver, E.; Said, K.; Poortmans, J.; Szlufcik, J.; Nijs, J. Improved anisotropic etching process for industrial texturing of silicon solar cells. *Sol. Energy Mater. Sol. Cells* **1999**, *57* (2), 179−188.
(24) Knight, S. C.; Unger, B. A.; Kolasinski, K. W. Crystallographically defined silicon macropore membranes. *Open Mater. Sci.* **2018**, *4* (1), 33−41.
(25) Choi, W.; Smits, J. G. A method to etch undoped silicon cantilever beams. *J. Microelectromech. Syst.* **1993**, *2* (2), 82−86.
(26) Ghajar, M. H.; Mousavi, M.; Burzhuev, S.; Irannejad, M.; Yavuz, M.; Abdel-Rahman, E. A short review on fabrication methods of micro-cantilever for ionic electroactive polymer sensors/actuators. *Int. J. Nanosci. Nanotechnol.* **2018**, *14* (2), 101−109.
(27) Sheeja, D.; Tay, B. K.; Yu, L. J.; Chua, D. H. C.; Milne, W. I.; Miao, J.; Fu, Y. Q. Fabrication of amorphous carbon cantilever structures by isotropic and anisotropic wet etching methods. *Diamond Relat. Mater.* **2003**, *12* (9), 1495−1499.
(28) Hein, A.; Dorsch, O.; Obermeier, E.Effects of metallic impurities on anisotropic etching of silicon in aqueous KOH-solutions. In *Proceedings of International Solid State Sensors and Actuators Conference (Transducers '97)*, **1997**; Vol. *1*, pp 687−690.
(29) Tanaka, H.; Abe, Y.; Yoneyama, T.; Ishikawa, J.; Takenaka, O.; Inoue, K. Effects of small amount of impurities on etching of silicon in aqueous potassium hydroxide solutions. *Sens. Actuator A Phys.* **2000**, *82* (1−3), 270−273.
(30) Monteiro, T.; Kastytis, P.; Gonçalves, L.; Minas, G.; Cardoso, S. Dynamic wet etching of silicon through isopropanol alcohol evaporation. *Micromachines* **2015**, *6* (10), 1534−1545.
(31) Pal, P.; Sato, K. A comprehensive review on convex and concave corners in silicon bulk micromachining based on anisotropic wet chemical etching. *Micro Nano Syst. Lett.* **2015**, *3* (1), 6.
(32) Rola, K. P.; Zubel, I. Investigation of Si(*hkl*) surfaces etched in KOH solutions saturated with *tertiary*-butyl alcohol. *J. Micromech. Microeng.* **2011**, *21* (11), 115026.
(33) Jiao, Q. B.; Bayanheshig; Tan, X.; Zhu, J. W.; Gao, J. X. The effects of ultrasound frequency and power on the activation energy in Si−KOH reaction system. *Chin. Chem. Lett.* **2014**, *25* (4), 617−620.
(34) Voss, R.; Siedel, H.; Baumgartel, H.Light-controlled, electrochemical, anisotropic etching of silicon. In *TRANSDUCERS '91:1991 International Conference on Solid-State Sensors and Actuators. Digest of Technical Papers*, **1991**; pp 140−143.
(35) Krah, T.; Büttgenbach, S.Surface structure of monocrystalline silicon anisotropically etched with the help of microwaves. In *Towards synthesis of micro-/nano-systems*; Springer: London, 2007; pp 337−338.
(36) Walczak, R.; Dziuban, J. A. Microwave enhanced wet anisotropic etching of silicon utilizing a memory effect of KOH activation—a remote E2MSi process. *Sens. Actuator A Phys.* **2004**, *116* (1), 161−170.
(37) Shikida, M.; Sato, K.; Tokoro, K.; Uchikawa, D. Differences in anisotropic etching properties of KOH and TMAH solutions. *Sens. Actuator A Phys.* **2000**, *80* (2), 179−188.
(38) Yang, C. R.; Chen, P. Y.; Chiou, Y. C.; Lee, R. T. Effects of mechanical agitation and surfactant additive on silicon anisotropic etching in alkaline KOH solution. *Sens. Actuator A Phys.* **2005**, *119* (1), 263−270.
(39) Aabdin, Z.; Xu, X. M.; Sen, S.; Anand, U.; Král, P.; Holsteyns, F.; Mirsaidov, U. Transient clustering of reaction intermediates during wet etching of silicon nanostructures. *Nano Lett.* **2017**, *17* (5), 2953−2958.
(40) Grau-Carbonell, A.; Sadighikia, S.; Welling, T. A. J.; van Dijk-Moes, R. J. A.; Kotni, R.; Bransen, M.; van Blaaderen, A.; van Huis, M. A. In situ study of the wet chemical etching of SiO_2 and nanoparticle@SiO_2 core−shell nanospheres. *ACS Appl. Nano Mater.* **2021**, *4* (2), 1136−1148.
(41) Jiang, Y.; Zhu, G.; Lin, F.; Zhang, H.; Jin, C.; Yuan, J.; Yang, D.; Zhang, Z. In situ study of oxidative etching of palladium nanocrystals by liquid cell electron microscopy. *Nano Lett.* **2014**, *14* (7), 3761−3765.
(42) Baraissov, Z.; Pacco, A.; Koneti, S.; Bisht, G.; Panciera, F.; Holsteyns, F.; Mirsaidov, U. Selective wet etching of silicon germanium in composite vertical nanowires. *ACS Appl. Mater. Interfaces* **2019**, *11* (40), 36839−36846.
(43) Gosálvez, M. A.; Sato, K.; Foster, A. S.; Nieminen, R. M.; Tanaka, H. An atomistic introduction to anisotropic etching. *J. Micromech. Microeng.* **2007**, *17* (4), S1−S26.
(44) Gosálvez, M. A.; Zubel, I.; Viinikka, E.Wet etching of silicon. In *Handbook of Silicon Based MEMS Materials and Technologies*, 2nd ed.; Elsevier: Boston, 2015; pp 470−502.

https://doi.org/10.1021/acsaelm.2c00824
ACS Appl. Electron. Mater. 2022, 4, 5191−5198

(45) Bangsaruntip, S.; Balakrishnan, K.; Cheng, S. L.; Chang, J.; Brink, M.; Lauer, I.; Bruce, R. L.; Engelmann, S. U.; Pyzyna, A.; Cohen, G. M.; Gignac, L. M.; Breslin, C. M.; Newbury, J. S.; Klaus, D. P.; Majumdar, A.; Sleight, J. W.; Guillorn, M. A. Density scaling with gate-all-around silicon nanowire MOSFETs for the 10 nm node and beyond. In *2013 IEEE International Electron Devices Meeting*, Washington, DC, U.S.A, **2013**; pp 20.22.21−20.22.24.
(46) Hur, S. G.; Yang, J. G.; Kim, S. S.; Lee, D. K.; An, T.; Nam, K. J.; Kim, S. J.; Wu, Z.; Lee, W.; Kwon, U.; Lee, K. H.; Park, Y.; Yang, W.; Choi, J.; Kang, H. K.; Jung, E.A practical Si nanowire technology with nanowire-on-insulator structure for beyond 10 nm logic technologies. In *2013 IEEE International Electron Devices Meeting*, Washington, DC, U.S.A, **2013**; pp 26.25.21−26.25.24.
(47) Veloso, A.; Huynh-Bao, T.; Rosseel, E.; Paraschiv, V.; Devriendt, K.; Vecchio, E.; Delvaux, C.; Chan, B. T.; Ercken, M.; Tao, Z.; Li, W.; Altamirano-Sánchez, E.; Versluijs, J. J.; Brus, S.; Matagne, P.; Waldron, N.; Ryckaert, J.; Mocuta, D.; Collaert, N.Challenges and opportunities of vertical FET devices using 3D circuit design layouts. In *2016 IEEE SOI-3D-Subthreshold Microelectronics Technology Unified Conference (S3S)*, Burlingame, CA, USA, **2016**; pp 1−3.
(48) Li, J.; Chen, C.; Jans, H.; Xu, X.; Verellen, N.; Vos, I.; Okumura, Y.; Moshchalkov, V. V.; Lagae, L.; Van Dorpe, P. 300 mm Wafer-level, ultra-dense arrays of Au-capped nanopillars with sub-10 nm gaps as reliable SERS substrates. *Nanoscale* **2014**, *6* (21), 12391−12396.
(49) Vos, I.; Hellin, D.; Vertommen, J.; Demand, M.; Boullart, W. Silicon nano-pillar test structures for quantitative evaluation of wafer drying induced pattern collapse. *ECS Trans.* **2011**, *41* (5), 189−196.
(50) Phillips, J. C.; Braun, R.; Wang, W.; Gumbart, J.; Tajkhorshid, E.; Villa, E.; Chipot, C.; Skeel, R. D.; Kalé, L.; Schulten, K. Scalable molecular dynamics with NAMD. *J. Comput. Chem.* **2005**, *26* (16), 1781−1802.
(51) Vanommeslaeghe, K.; Hatcher, E.; Acharya, C.; Kundu, S.; Zhong, S.; Shim, J.; Darian, E.; Guvench, O.; Lopes, P.; Vorobyov, I.; Mackerell, A. D. CHARMM general force field: A force field for drug-like molecules compatible with the CHARMM all-atom additive biological force fields. *J. Comput. Chem.* **2009**, *31* (4), 671−690.
(52) Yu, W.; He, X.; Vanommeslaeghe, K.; MacKerell, A. D. Extension of the CHARMM general force field to sulfonyl-containing compounds and its utility in biomolecular simulations. *J. Comput. Chem.* **2012**, *33* (31), 2451−2468.

Recommended by ACS

Controllable Synthesis of Large-Scale Monolayer MoS_2 Dendritic Flakes with Serrated Edges and Their Multimodal Microscopy and AFM Characterizations

Fei Chen, Yajie Li, *et al.*

JULY 28, 2022
THE JOURNAL OF PHYSICAL CHEMISTRY C

READ

Role of Hydrogen in Suppressing Secondary Nucleation in Chemical Vapor-Deposited MoS_2

Sayema Chowdhury, Sanjay K. Banerjee, *et al.*

DECEMBER 13, 2022
ACS APPLIED ELECTRONIC MATERIALS

READ

Real-Time Study of Surface-Guided Nanowire Growth by *In Situ* Scanning Electron Microscopy

Amnon Rothman, Ernesto Joselevich, *et al.*

OCTOBER 28, 2022
ACS NANO

READ

Sawtooth Faceting in Rutile Nanowires

Ping Zhou, Guo-zhen Zhu, *et al.*

MARCH 16, 2022
ACS OMEGA

READ

Get More Suggestions >

https://doi.org/10.1021/acsaelm.2c00824
ACS Appl. Electron. Mater. 2022, 4, 5191−5198